# Influence of Internal Channel Geometry of Gas Turbine Blade on Flow Structure and Heat Transfer

**Ryszard Szwaba, Piotr Kaczynski, Janusz Telega, Piotr Doerffer**

Institute of Fluid-Flow Machinery, Polish Academy of Sciences (IMP PAN), Fiszera 14, 80-952 Gdansk, POLAND

This paper presents the study of the influence of channel geometry on the flow structure and heat transfer, and also their correlations on all the walls of a radial cooling passage model of a gas turbine blade. The investigations focus on the heat transfer and aerodynamic measurements in the channel, which is an accurate representation of the configuration used in aeroengines. Correlations for the heat transfer coefficient and the pressure drop used in the design of internal cooling passages are often developed from simplified models. It is important to note that real engine passages do not have perfect rectangular cross sections, but include a corner fillets, ribs with fillet radii and a special orientation. Therefore, this work provides detailed fluid flow and heat transfer data for a model of radial cooling geometry which has very realistic features.

**Keywords: cooling, internal blade channels, aerodynamics with heat transfer**



## Introduction

Heat exchange is a critical issue in the development of gas turbine blades. Gas temperature at the first stage of the turbine is extremely high and can cause metal melting, thus, intensive cooling of the first blades is absolutely necessary. Usually a combination of internal convection cooling and film cooling is applied. They have to be designed for high efficiency, long life cycles and safe operation in spite of being exposed to high aerothermal loadings of the engine.

The internal cooling systems of high pressure blades in modern aero engines are very complex and essentially rely on serpentine systems. The data available for design purposes tends to be in the form of correlations obtained from a large number of idealized geometries, e.g. [1, 2, 3] over restricted ranges of operation. The work described in the present paper is a part of the work undertaken within the EU ERICKA project [4]. The project concerning generation of test data on the heat transfer and pressure drop performance of ribbed cooling passages which, together with CFD and optimization tools, is intended to support the development of more effective cooling systems for rotating turbine components.

In order to enable the turbine to operate at high temperatures, the gas-swept components are cooled by air drawn from the compressor. One of the ERICKA project objectives [4] was to increase the aircraft engine efficiency modifying the cooling system of turbine blades. There are two kinds of approaches to this problem, schematically indicated in Fig. 1. One of the ways is an increase in the turbine entry temperature (TET) of 50K what can improve the SFC if the turbine cooling flow is not altered. The maximum permissible turbine entry temperature is set by technologies including thermal barrier coatings, blade materials and the cooling system design. This means that, if the blade technology is not enhanced, an increase in the TET is normally accompanied by an

**Nomenclature**

| | | | |
|---|---|---|---|
| X | channel length (mm) | P0 | inlet stagnation pressure (Pa) |
| Y | channel height (mm) | PP | stagnation pressure (Pa) |
| Z | channel span (mm) | HTC, h | heat transfer coefficient |
| Nu | Nusselt number | LE | leading edge |

| | | | |
|---|---|---|---|
| Re | Reynolds number | TE | trailing edge |
| d | diameter (mm) | PS | pressure side |
| T | temperature (K) | SS | suction side |
| k | material constant | TET | Turbine Entry Temperature |
| U | velocity (m/s) | **index** | |
| U_m | mean velocity (m/s) | *W* | Wall |
| f | frequency (Hz) | *G* | Gas |
| t | time (s) | *i* | initial condition |
| SFC | Specific Fuel Consumption | *aw* | adiabatic wall |

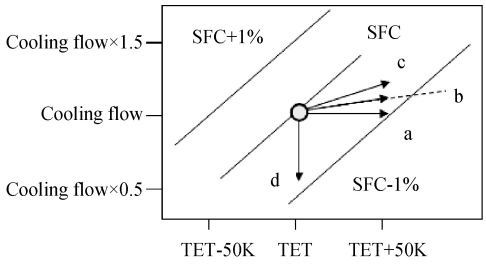


**Fig. 1** Schematic diagram indicating the benefits of improved cooling technology on SFC [4]

increase in the cooling flow and the latter acts to reduce the fuel efficiency.

Another way to increase the aircraft engine efficiency, which is a part of the research presented in this paper, is reducing the cooling pressure drop whilst maintaining the same peak cycle temperature. The vertical line, d, in the Figure indicates how this would reduce the SFC. For a fixed turbine entry temperature, a reduction in the amount of cooling flow improves the cycle efficiency. In practice, it is likely that the improved cooling technology will be used in new designs to both reduce the cooling flow relative to the flow required for the existing technology and increase the TET.

The main goal of this paper is to study the influence of channel geometry on the flow structure and heat transfer, and also their correlations on all the four walls of a radial cooling passage model of a gas turbine blade.

The basic (reference) configuration of the measurement channel characterizes the 1:4 cross section aspect ratio and parallel settings of ribs on the upper and lower walls. Based on the reference channel, a modification direction of this configuration is proposed to enhance the aerodynamics performance, i.e. to achieve a lower pressure drop what will directly result in lower aerodynamic losses.

The result of the channel modification idea is shown in Fig. 2 and it has been also confirmed by CFD simulations [5]. As one can see parallel ribs (Fig. 2a) generate two counterrotating vortices. Changing the inclination of ribs on the opposite wall (Fig. 2b) the so called crossing setting of ribs in the channel is received. This rib configuration may create the air motion in the channel, flowing over the whole circumference tending to provoke one main vortex and in this way to reduce the mixing processes in the channel what can have an effect on a decrease in losses.

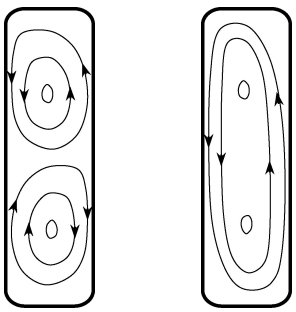


**Fig. 2** Rib setting effect on channel flow, (a) parallel ribs, (b) crossing ribs

Correlations for the heat transfer coefficient and pressure drop used in the design of radial cooling passages are often developed from data gained from simplified, flat surfaced models over specific conditions [6]. It is important to note that real engine passages do not have perfect rectangular cross sections, but include fillets and space oriented ribs also with fillet radii. Therefore, this work provides detailed fluid flow and heat transfer data for a model of radial cooling geometry which has very realistic features. The ribs are of a real shape.

The experimental setup presented here is able to provide complementary data of the heat transfer and the flow pattern in a cooled inner channel of a turbine blade with two different geometries (rib settings). The flow structure and pressure drop were measured by means of the classical measurements techniques. The stagnation pressure and velocity were measured in the channel outlet plane. The Transient Liquid Crystal method was used to investigate the heat transfer. This measurement technique is

well known and has been successful in high resolution heat transfer measurements on surfaces with complex shapes and geometries [7, 8, 9]. The method allows obtaining detailed surface distributions of local heat transfer coefficients in cooled channels, whereby it is possible to predict the result of the heat load under real-engine conditions. One of the advantages of this method is that there is no need to reach stable conditions in the wall temperature, what is very important in the studies where duct geometry has a large surface and a highly curved and complex flow structure.

## Experimental Setup

### Heat transfer measurements

The heat transfer measurements were done by means of the TLC (Transient Liquid Crystal) measurement technique [10, 11]. Liquid crystals can be in the form of a sheet or sprayable microencapsulated water slurries placed on the wall of a test section. In this experiment a narrow band liquid crystal sheet (R35C1W) was used. The first step was the calibration which determined the temperature at which the green color band of liquid crystal gives the highest intensity. In the transient method the green color is investigated because its distribution versus temperature shows a very clear, well defined peak. More details of the calibration process are described in [12].

The test section was also equipped with thermocouples which measure the temperature along the flow and on the channel walls. The heat flux was triggered due to the temperature difference between the gas and the channel walls. In this experiment hot air was introduced into the channel triggering the heat transfer from the flowing gas to the surfaces of the channel walls. Over time, the liquid crystals located on the wall surface were heated up and finally changed their color. Knowing the material properties of the channel walls, the local temperatures and also the time which passed from the start of the measurement (i.e. the moment of introduction of hot air into the channel) to reach the wall temperature activating the green color, one can determine the heat transfer coefficient. The 3CCD camera recorded images during the measurement to determine time $t$ at which the green intensity peak was achieved. The recorded frames were analyzed by means of our own automated MATLAB code. The software [13] for searching the time of the green intensity peak in every pixel was developed. Having the above information it was possible to determine the distribution of the heat transfer coefficient $h$ on particular walls.

### Test section

The view of the measurement test section is shown in Fig. 3. This test section corresponds to an internal radial passage channel of a turbine blade. The lower and upper walls are ribbed, what corresponds to the pressure and suction side of the turbine blade inner channel. In the downstream view the left side wall corresponds to the leading edge direction, the right side wall corresponds to the trailing edge direction. The following measurements were carried out during the tests:

- stagnation pressure and temperature at the inlet
- boundary layer profile (stagnation pressure) upstream of the ribbed section
- static pressure distribution along the channel
- stagnation and static pressure distribution in the cross-section downstream of the ribbed section
- velocity distribution in the cross-section downstream of the ribbed section by means of HWA (hot wire anemometry)
- heat transfer on all four walls of the measurement channel.

All measured pressures in the test section, both static and stagnation, were measured by means of a pressure scanner - PSI NetScaner 9116 with a range 2500 Pa. The measurement accuracy of the scanner is ±1.5 Pa.

Two configurations of the test section shown in Fig. 3 were used in the experiment. These two channels differ in terms of the setting of ribs on the lower and upper walls. One setting is shown in Fig. 3a. In this configuration the direction of ribs on the lower and upper wall is the same. The number of ribs on the lower wall and on the upper wall is 25 and 24, respectively. Hence, the ribs on the upper wall are shifted half a pitch (10 mm) in relation to the lower wall. In the projection view on the lower wall the ribs will be parallel.

The second configuration of the test section is shown in Fig. 3b. In this setting the direction of ribs on the lower and upper walls is different. The number of ribs on the lower and upper walls is the same, namely 25. Thus, in the projection view the ribs will be crossing on the lower wall.

In addition to the two configurations of ribs, two different Reynolds numbers (Re=63 000 and 120 000) were taken in account in the experiment. Together it gives 4 measurement cases, and the nomenclature for particular cases which will be used in the paper is shown in Table 1.

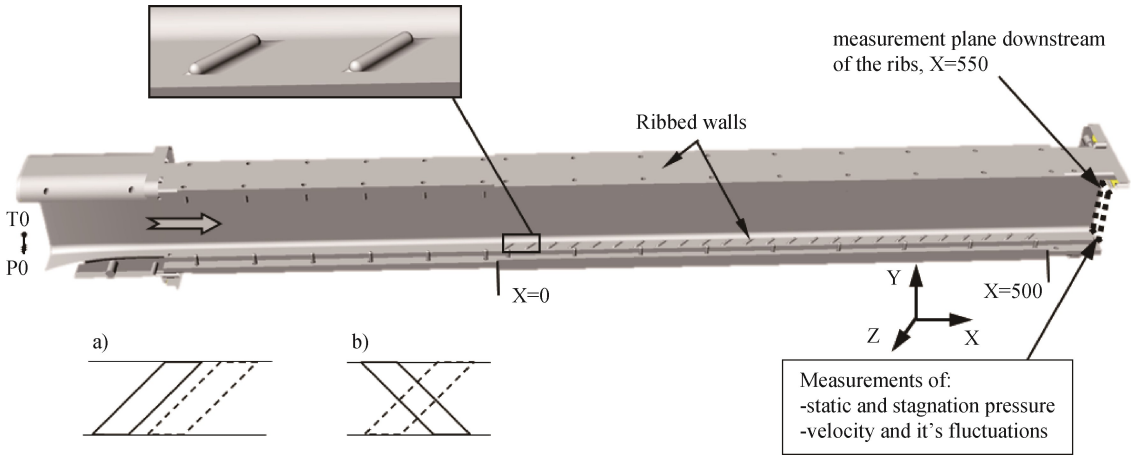


**Fig. 3** View of test channel

**Table 1** Measurement cases and nomenclature

| Rib setting | Reynolds Number | |
|---|---|---|
| | 63 000 | 120 000 |
| Parallel | Par-63k | Par-120k |
| Crossing | Cr-63k | Cr-120k |

Small ribs located on one single wall have a parallel setting (Fig. 3) to each other. The ribs were skewed by 45° in relation to the flow direction. The pitch of the ribs was 20 mm. The aspect ratio of the channel was 1:4. The Reynolds number in the experiment given in the table is based on the hydraulic diameter of the channel flow.

The test section scheme together with the system of hot air preparation is presented in Fig. 4. The ambient air enters through the heater placed at the inlet of the settling chamber. Hot air is permanently evacuated from the settling chamber through the test section or the bypass system. While the bypass valve is open, the air from the settling chamber flows to the bypass circuit. This arrangement is for establishing the mass flow and temperature, the same as during the measurement. When the bypass valve is closed, the main valve is open and hot air flows through the test section and then to the vacuum tank. The mass flow rate in the test section is controlled during the measurements by the orifice plate. To investigate the heat transfer, liquid crystal sheets were placed on the surface of the inner walls of the test section.

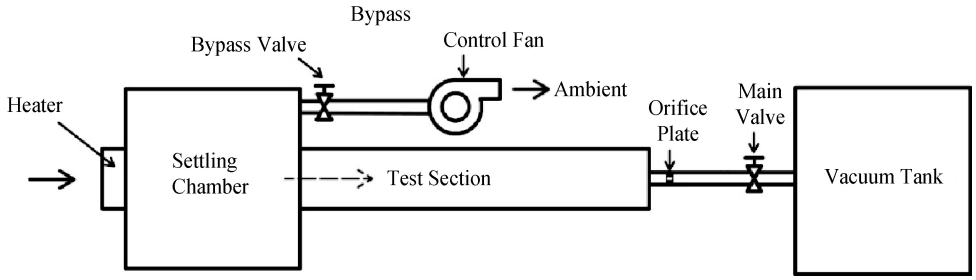


**Fig. 4** Measurement system scheme

The imaging system allows observing three walls simultaneously, one sidewall and two ribbed walls (see Fig. 5). Two flat mirrors are mounted at 30 degrees and show upper and lower ribbed walls. Illumination is provided by four strip LED lamps. The white color of light and its precise orientation gives sufficient response of the green signal from the narrow band liquid crystal sheet. The imaging system comprises 3 CCD cameras which record images at a rate of 30 Hz and with a resolution of 1024x768 pixels.

The local heat transfer coefficient is calculated in every pixel separately by solving the analytically unsteady, one dimensional conduction equation with the assumption of a semi-infinite wall for the whole of the test period, constant initial temperatures and a convective boundary condition. For this purpose a MATLAB code was specially created to calculate the heat transfer coefficient $h$ from the equation (1) developed by Clifford and Jones [10]. The MATLAB code is used to calculate the heat transfer coefficient at each pixel location by comparing the experimental green intensity history with the gas temperature flowing through the test section. At the beginning the software calculates time $t$ after which there is the maximum intensity of the green color for every

pixel separately. Then, using gas temperature $T_{G,aw}$ measured by four thermocouples placed along the channel (linearly averaged) the local heat transfer coefficient is calculated. $T_{W,lc}$ is the wall surface temperature at which liquid crystal adopts the green color. $T_i$ is the initial wall temperature (constant during measurements) while $k$ is a product of the channel material density, specific heat and thermal conductivity.

$$\frac{T_{W,lc}-T_i}{T_{G,aw}-T_i}=1-\exp(h^2\frac{t}{k})erfc(h\sqrt{\frac{t}{k}}) \quad (1)$$

erfc(z)=(2/√∏)∫e dt

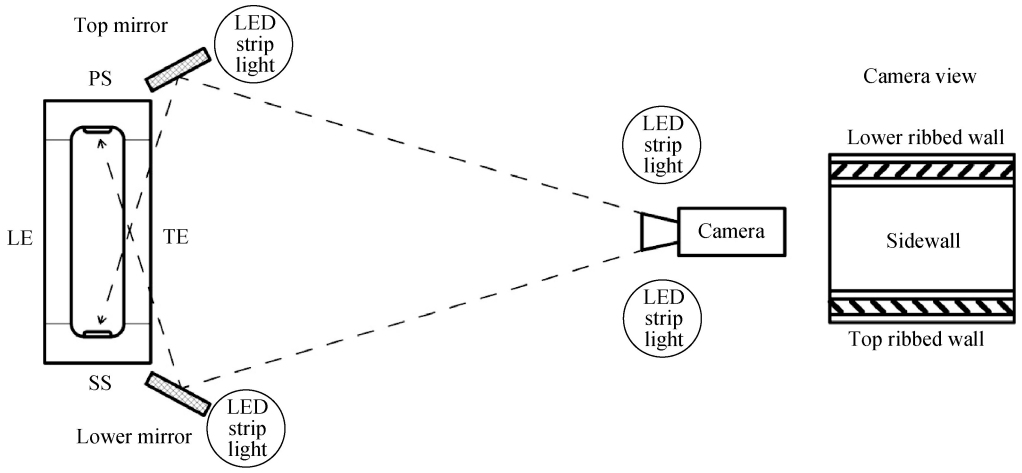


**Fig. 5** Image system scheme

## Results and Discussion

### Pressure measurements

The normalized stagnation pressure distribution at the test section outlet plane (X=550, Fig. 3) is shown in Fig. 6. The results are shown according to the downstream view. The stagnation pressure was measured by means of a miniature Pitot probe, 60 mm downstream of the ribs. The coordinates Y = 0 and Z = 0 are assumed in the middle of the rectangular channel as is shown in the Figure.

Fig. 6 shows a comparison of pressure distribution for two different rib configurations and for the same Reynolds number, Re=63000. These measurements show that a pair of main vortices is created in the flow by the ribs. The dashed ellipses with an arrow show the sense of rotation of the induced vortices. The parallel setting of ribs (Fig. 6a) in the channel creates two main vortices with the opposite sense of rotation, but the flow direction in these two vortices is the same in the channel centre, it is passing from one side wall to the other. The second, crossing setting of the ribs (Fig. 6b) creates a different pattern in the flow, i.e. two main vortices with same sense of rotation, but the flow direction in these two vortices near the channel center is opposite. In Fig. 6 one can also notice that regions of higher stagnation pressure are located near the upper and lower walls, where the flow forced by the skewed ribs goes down over the rib toward the side wall. For the higher Reynolds number the obtained results are very similar, except for the pressure drop which is about 2% deeper.

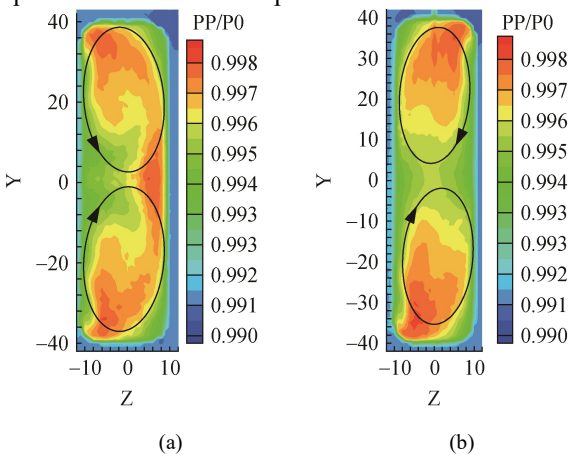


**Fig. 6** Normalized stagnation pressure downstream of ribbed section, (a) Par 63k, (b) Cr-63k

In Table 2 the flow losses at the outlet of the ribbed channel are shown. The losses are integrated on the whole plane at X=550 with a range Y = -38 ÷ 38 and Z = -9 ÷ 9. The loss coefficient $\zeta$ was calculated according to Eq. 2, which means the losses of stagnation pressure normalized by the dynamic component of the flow.

$$\zeta=\frac{P0-PP}{0.5\rho_{out}U_{out}^2} \quad (2)$$

Basing on Table 2 one can see the tendency of decreasing normalized losses $\zeta$ in case of the crossing rib configuration, while the total pressure drop remains almost the same for both rib configurations. Such results

show that in the case of crossing ribs, at the same total pressure drop as in a parallel rib case, the dynamic processes in the flow producing losses are slightly weaker and an average velocity in the whole cross section is a little bit higher in relation to parallel ribs in the flow. The difference is higher in case of a lower Reynolds number, in case of higher *Re*, the tendency of losses decreasing for crossing ribs gets weaker.

**Table 2** Losses at the outlet of the ribbed channel

| Re [-] | Loss coefficient ζ | |
|---|---|---|
| | Parallel | Crossing |
| 63k | 0.85 | 0.82 |
| 120k | 0.83 | 0.82 |

### Velocity and its fluctuations measurements

The velocity measurements downstream of the ribbed section were also a part of the investigation campaign. The velocity distribution was measured in the same cross-section as the pressure measurements, namely 60 mm downstream of the ribs at X=550. The measurements were performed by means of a hot wire probe, hence, in this case the results show the velocity magnitude. The *X* component (longitudinal velocity) is dominating in the channel flow.

Fig. 7 shows a comparison of the stagnation pressure and the velocity distribution for the same flow case, Par-63k. In this Figure one can notice that regions of higher velocity correspond to regions of higher stagnation pressure. The highest flow velocity is in areas near the upper and lower walls, where the flow goes down over the rib toward the LE side wall. The region of high velocity is also observed in the middle of the channel near the TE side wall, to which the flow in the vortices is directed.

In Fig. 8 one can see a comparison of the velocity distribution for the same Reynold number, Re=120k, but for a different rib setting. In this Figure, in addition to the different vortex pattern between two rib settings, one can also observe a small flow asymmetry in Fig. 8b between the suction and pressure sides (near upper and lower walls). There is a little higher longitudinal velocity region (darker red) near the suction side. Higher velocity means lower losses in the flow what is also confirmed by Table 2. This results partly confirm the assumption made in the introduction that the crossing ribs introducing the circumferential motion in the whole channel can decrease the flow losses, but such configuration seems to be more adequate for lower channels (lower aspect ratio, e.g. 1:3 or 1:2). For such channels the circumferential motion should be stronger and could be seen more clearly in the pressure and velocity distribution, also the lower pressure drop would be more noticeable. Nevertheless, for crossing setting of ribs (Fig. 8b) the week circumferential motion comprising two dominant vortices is started (also confirmed by numerical simulations, [5]). The flow direction in two main vortices at the channel center is opposite. The part of the mass flow is "trying" to find the way of lower resistance, starts to direct along the side walls, beginning the circumferential motion. There is also the other side of the coin, how the pressure drop influences the heat transfer. This aspect will be described in the next paragraph.

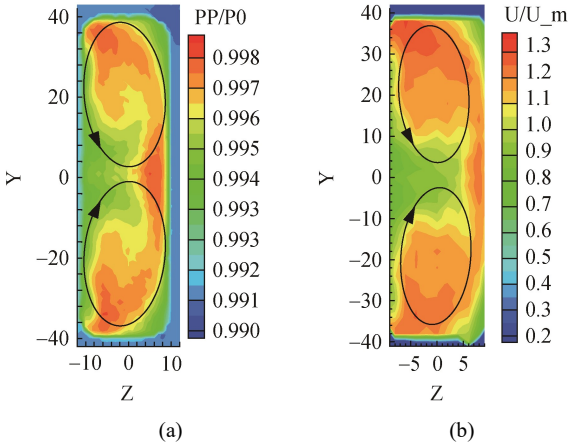


**Fig. 7** Measurement plane downstream of ribbed section, (a) normalized stagnation pressure, (b) velocity magnitude

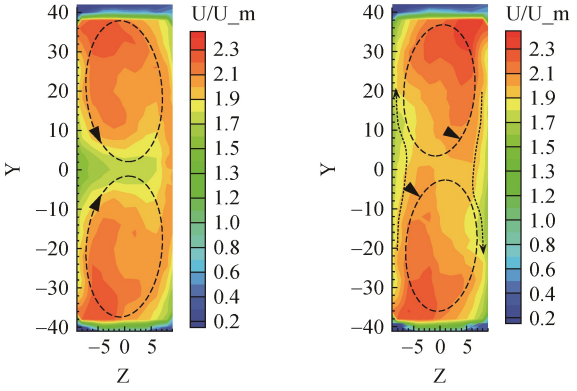


**Fig. 8** Velocity distribution in the plane downstream of ribbed section, (a) Par-120k, (b) Cr-120k

The results of the velocity fluctuations measured by means of hot wire anemometry for two different flow Reynolds numbers and for parallel rib settings are shown in Fig. 9. The measurement plane was located downstream of the ribbed section at X=550, in the same plane adequate for the velocity and stagnation pressure measurements.

The results in Fig. 9 show that the lowest level of the velocity fluctuations in the flow can be observed in the acceleration regions near the bottom and upper walls of the channel. The highest velocity fluctuations are ob-

served near the side walls in areas where the flow decelerates. Generally, we can say that a high level of turbulence can be observed in the channel with the aspect ratio 1:4, which is relatively narrow. The average turbulence intensity in case of a lower *Re* number is at a level of about 10%. An increase in the turbulence level with respect to the smooth channel with the same geometry is around 80%. A high level of turbulence on the one side supports the heat exchange, but on the other side slightly increases the losses in the channel flow.

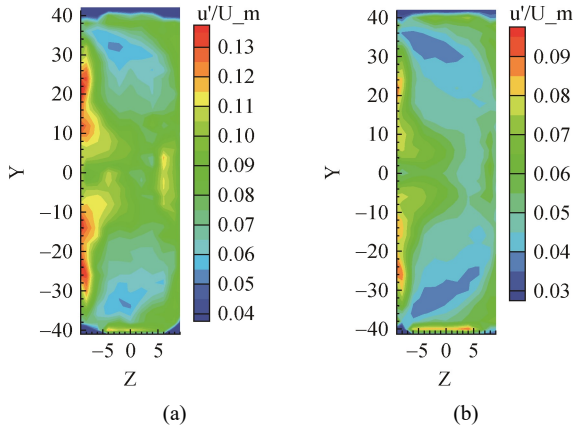


**Fig. 9** Normalized velocity fluctuations distribution in the plane downstream of ribbed section, (a) Par-63k (b) Par-120k

The type of rib configuration in the channel almost does not have any effect on the average turbulence level in the channel, the parallel and crossing setting of ribs characterizes a similar maximal and minimal level of velocity fluctuations. Comparing the results for two different Reynolds numbers (Figs. 9a and 9b) one can say that the relative (normalized) velocity fluctuations decreased about a quarter for higher Reynolds numbers in comparison to lower numbers. This shows that the turbulence does not scale in the same way as the increase in velocity.

**Heat transfer measurements**

Fig. 10 presents the heat transfer coefficient distribution on all the four channel walls for the Par-63k flow case. The flow structure coming from aerodynamic measurements is placed on the right side. Arrows on the pressure distribution plane indicate the location in the space of particular walls.

Fig. 10 shows that the *HTC* distribution is highly correlated with the flow structure. The heat transfer strongly increases in areas where the stagnation pressure and velocity are high. The stagnation pressure is higher in the middle of the TE side wall than on the LE wall. This is reflected in the *HTC* distribution, in the middle of the duct, the *HTC* on the trailing edge wall (TE) is higher in relation to the leading edge wall. A correlation between pressure (velocity) and the heat transfer coefficient is also seen on the ribbed walls and in those channel corners where the flow has accelerated. The higher pressure (velocity) in the left corners (at the leading edge wall) is observed, thus, in these regions one can see very high values of the heat transfer coefficient, in contrast to the opposite corner where *HTC* values are much lower.

Generally, one can say that the heat transfer is higher in regions where shear stresses increase (Reynolds analogy). The shear stresses increase and the heat transfer coefficient also significantly increases just downstream of the rib where the flow driven by the vortex goes down. The heat transfer radically decreases in the region before the ribs where the flow separates.

Watching the *HTC* distribution on the leading edge side wall (Fig. 10) one can also observe the phenomenon of development of vortices along the channel. At the inlet where the ribs start to influence the flow the height of two main vortices is small, then, one can see that they gradually enlarge along the channel. Finally, at the outlet, the vortices occupy the whole cross-section of the channel.

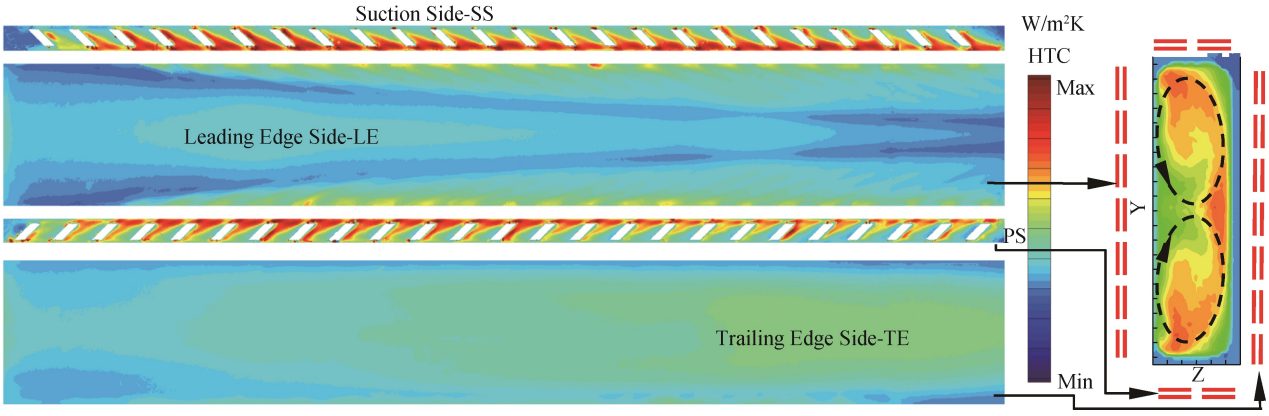


**Fig. 10** Heat transfer coefficient distribution on all channel walls for Par-63k flow case

The averaged normalized Nusselt number (Nu/Nu0) distributions along the channel for side and ribbed walls and for different flow cases are shown in Figs. 11÷13. For side walls the averaging was made calculating the mean value, vertically line by line along the channel. For the ribbed walls the Nusselt number was calculated averaging the surface between the neighboring ribs.

Figs. 11 and 12 show that the heat exchange increases on the side walls along the channel from the inlet to about 80% of the duct length. At the outlet the average Nusselt number values start to decrease. The parallel setting of ribs causes the difference in the *Nu* distribution between the LE and TE walls. On the LE wall, where the direction of vortices is out from the wall (see Fig. 10), lower average Nusselt number values in relation to the TE wall are observed. For the crossing rib setting, where the pressure distribution at the side walls is very similar, also the *Nu* distribution on the LE and TE walls is very similar.

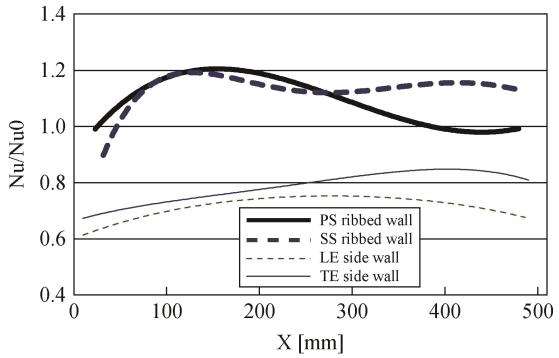


**Fig. 11** Averaged normalized Nusselt number distribution on channel walls for Par-63k flow case

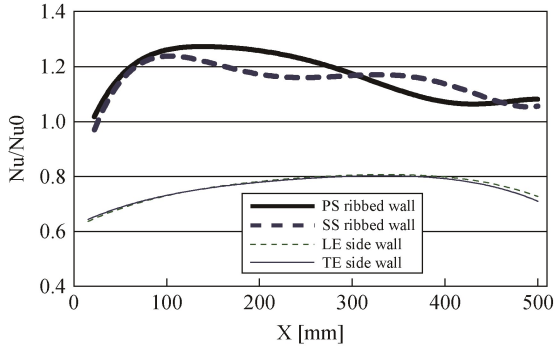


**Fig. 12** Averaged normalized Nusselt number distribution on channel walls for Cr-63k flow case

Figure 11 and 12 also show the heat exchange along the ribbed walls on the pressure and suction sides. In these Figures one can see that the heat transfer increases quickly from the very beginning, what is due to the development of vortices in the channel. When the vortices have developed, the average *Nu* stabilizes, further downstream of the channel there is a small tendency in the average heat exchange to be decreasing in the direction of the duct outlet. The vortices generated by the ribs significantly increase the heat exchange on the walls. The averaged Nusselt number values on the ribbed walls are approximately 50÷80% higher in relation to the side walls.

For the Par-63k flow case (Fig. 11), at the outlet of the channel one can also observe the difference in the heat transfer between the suction (SS) and pressure (PS) sides. The reason for this phenomenon is a non-uniform velocity distribution in the channel. On this example one can also conclude that the heat transfer can change due to the local small asymmetry of the flow field. A similar situation can be observed in the case of a higher Reynolds number, Re=120k (Fig. 13) where the heat transfer on the suction side for the Cr-120k flow case is weaker from the very beginning. If we look at the velocity distribution for this flow case (Fig. 8b) one can observe that near the suction side (upper ribbed wall) the velocity magnitude is a little bit higher in relation to the opposite, pressure side wall and also in relation to the suction side of the parallel rib configuration. As Fig. 8 shows the longitudinal component of the velocity this could mean that the flow accelerating in one direction gets weaker in other directions (perpendicular to the main flow), but in consequence, the surface stresses and the heat transfer also get down. A positive effect of such phenomenon (increase in the longitudinal velocity) is a decrease in losses, but from the heat transfer point of view it is not a promising perspective as a simultaneous decrease in losses in the channel and keeping the heat transfer on the same level can be very difficult to fulfill.

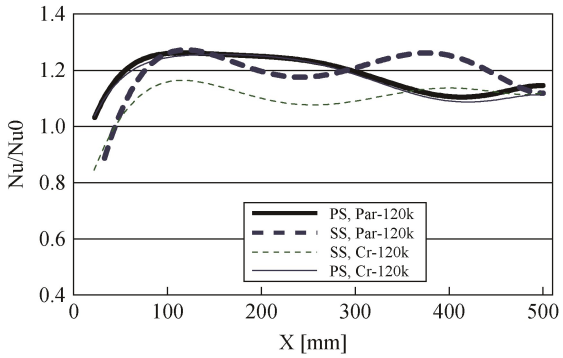


**Fig. 13** Averaged normalized Nusselt number distribution on channel walls for Par-120k and Cr-120k flow cases

## Conclusions

A test section has been developed and designed to obtain a similar flow pattern as in the reference inner cooled channel of a turbine blade. The test channel has the same aspect ratio and shape of the ribs. The following conclusions can be drawn from the above described

investigations:

- The heat transfer was compared with the aerodynamic measurement (flow pattern) in the ribbed channels;
- Ribs on the suction and pressure side walls create a specific flow structure with two dominant vortices along the channel with the sense of rotation depending on the configuration of ribs;
- The basic channel modification to the crossing rib configuration shows a tendency towards decreasing losses. This solution should be more adequate for lower aspect ratios;
- A high level of turbulence in the ribbed and narrow channels was observed. The turbulence level decreased with the growing Reynolds number;
- The heat transfer coefficient distribution on the walls is highly correlated with the vortex pattern and the stagnation pressure distribution in the channel;
- The heat transfer strongly increases in areas where local velocity (stagnation pressure) is higher. Generally, there is a higher heat transfer in regions where shear stresses increase;
- In the radial cooled passage channel of the turbine blade the differences in the heat transfer between the suction and pressure sides can appear due to the local small asymmetry of the flow field.

Summarizing, the positive slight tendency towards decreasing losses in case of the crossing rib configuration was observed, but the perspectives are not promising with respect to the heat transfer results as decreasing the channel flow losses may be followed by the heat transfer downgrade conditions. Further research is needed to provide more detailed explanation of such behavior of the flow.

## Acknowledgement

The research leading to these results has received funding from the European Union Seventh Framework Programme (FP7/2007-2013) under Grant Agreement No. 233799 (ERICKA). Permission for publication is gratefully acknowledged by the authors.

## References

[1] Metzger D. E., Larson D. E., Use of Melting Point Surface Coating for Local Convection Heat Transfer Measurements in Rectangular Channel Flows with 90-deg Turns, ASME Journal of Heat Transfer, Vol. 108, pp. 48–54, (1986)

[2] Kiml R., Mochizuki S., Murata A., Effects of Rib Arrangements on Heat Transfer and Flow Behavior in a Rectangular Rib-Roughened Passage: Application to Cooling of Gas Turbine Blade Trailing Edge, ASME Journal of Heat Transfer, Vol. 123, pp. 675–681, (2001)

[3] Arts T., Benocci C., Rambaud P., Experimental and Numerical Investigation of Flow and Heat Transfer in a Ribbed Square Duct, 3rd International Symposium on Integrating CFD and Experiments in Aerodynamics, U.S. Air Force Academy, Colorado, (2007)

[4] http://www.ericka.eu, (2009-2014)

[5] Kaczyński P., Szwaba R., Doerffer P., Flaszyński P., Aerodynamic Enhancement in Inner Channel of Turbine Blade, Task Quarterly Vol. 19, No 2, pp. 101–110 (2015)

[6] Cakan, M., Aero-thermal Investigation of Fixed Rib-roughened Internal Cooling Passages, Ph.D. Thesis, Turbomachinery Department, Von Karman Institute for Fluid Dynamics, Brussels, (2000)

[7] Irland P. T., Jones T. V., The Measurement of Local Heat Transfer Coefficients in Blade Cooling Geometries, AGARD Conference on Heat Transfer and Cooling in Gas Turbines, CP 390 Paper 28, Bergen, (1985)

[8] Jones T. V., Hippensteele S. A., High Resolution Heat Transfer Coefficient Maps Applicable to Compound Curve Surfaces Using Liquid Crystals in a Transient Wind Tunnel, NASA TM 89855, (1988)

[9] Vogel G., Graf A. B. A., Wolfersdorf J., Weigand B., A Novel Transient Heater-Foil Technique for Liquid Crystal Experiments on Film-Cooled Surfaces, ASME Journal of Turbomachinery, Vol. 125, pp. 529–537, (2003)

[10] Clifford R. J., Jones T. V., Dunne S. D., Techniques for Obtaining Detailed Heat Transfer Coefficient Measurements within Gas Turbine Blade and Vane Cooling Passages, ASME Paper 83-GT-58, Arizona, USA, (1983)

[11] Ireland, P.T., Neely, A.J., and Gillespie, D.R.H., Turbulent heat transfer measurements using liquid crystals, International Journal of Heat and Fluid Flow, Vol.: 20, Issue: 4, pp. 355–367, (1999)

[12] Szwaba R., Kaczyński P., Doerffer P., Telega J., Flow Structure and Heat Exchange Analysis in Internal Cooling Channel of Gas Turbine Blade, Journal of Thermal Science Vol.25, No.4, pp. 336–341, (2016)

[13] Telega J., Doerffer P., Szwaba R., Kaczyński P., Parallelized Numerical Code For Derivation Of Heat Transfer Coefficient From Experimental Data, TASK Quarterly, Vol. 19, No. 2, pp. 197–205, (2015)